Supporting Information

1. Experimental Section

Materials. PM6 batches with different molecular weights and Y6 were synthesized in our group. L8-BO, N3, BTP-2F-ThCl and PFN-Br were purchased from Solarmer Materials Inc. Solvents were dried and distilled from appropriate drying agents prior to use.

Device Fabrication and Testing. All the devices were fabricated in the normal architecture. These substrates were cleaned in water, acetone, and isopropyl alcohol. After drying, the substrates were spin-coated with 40 nm PEDOT:PSS (purchased from Xi'an Polymer Light Technology Corp.). The photovoltaic layer was blade-coated in the air from a solution of PM6:Y6 (1:1.2, 5 wt% $PM6_L$) with different solution concentrations (14.0 mg mL^{-1}; 12.0 mg mL^{-1}; 10.0 mg mL^{-1}; 8.0 mg mL^{-1}; 6.8 mg mL^{-1}; 6.5 mg mL^{-1}; 6.3 mg mL^{-1}; 6.0 mg mL^{-1}) in chloroform. In addition, the PM6:Y6 blend was blade-coated from a solution of PM6: Y6 (1:1.2, wt%) with different concentrations (14.0 mg mL^{-1}; 12.0 mg mL^{-1}; 10.0 mg mL^{-1}; 8.0 mg mL^{-1}; 6.8 mg mL^{-1}; 6.5 mg mL^{-1}; 6.3 mg mL^{-1}; 6.0 mg mL^{-1}) in chloroform. Besides, the other three photovoltaic layers, consisting of three different photovoltaic systems (PM6:L8-BO, PM6:N3, and PM6:BTP-2F-ThCl) without and with the of $PM6_L$ (5 wt%) additives were dissolved in chloroform and subsequently bladed on top of PEDOT:PSS layer. A PFN-Br (poly[(9,9-bis(3'-((N,N-dimethyl)-N-ethylammonium)-propyl)-2,7-fluorene)-alt-2,7-(9,9-dioctylfluorene)]dibromide) layer *via* a solution concentration of 0.5 mg mL^{-1} was deposited the top of active layer. Finally, the top argentum electrode of 100 nm thickness was thermally evaporated (Suzhou Fangsheng FS-300) through a mask onto the cathode buffer layer under a vacuum of$\sim 5\times10^{-6}$ mbar. The typical active area of the investigated devices was 5 mm^2. The current-voltage characteristics of the solar cells were measured by a Keithley 2400 source meter unit under AM1.5G (100 mW

cm^{-2}) irradiation from a solar simulator (Enlitech model SS-X160R). Solar simulator illumination intensity was determined at 100 mW cm^{-2} using a monocrystalline silicon reference cell with KG5 filter. Short circuit currents under AM1.5G (100 mW cm^{-2}) conditions were estimated from the spectral response and convolution with the solar spectrum. The external quantum efficiency was measured by a Solar Cell Spectral Response Measurement System QE-R3011(Enli Technology Co., Ltd.).

Large-scale solar module fabrication. For the large-scale organic solar modules (5.0 cm × 5.0 cm), the dopant-free and $PM6_L$-based active layers were achieved using the above-mentioned methods. When fabricating the lager-area organic modules, the square ITO was patterned by laser ablation. After PEDOT:PSS was deposited, active layer was coated through a doctor blade. After PFN-Br layer was deposited, then the femtosecond laser (Coral GR12W-50K, Suzhou Microtreat Intelligent Technology Co., Ltd) with 532 fs pulse width was utilized to pattern the active layer (P2 line) for cell-to-cell connection and separate each sub-cell (P3 line) after the deposition of Ag. The femtosecond laser would not damage ITO in the bottom, and it would assist to form good contact between sub-cells.

Material characterization. The molecular weights of various PM6 batches were estimated by high-temperature gel permeation chromatography (HT-GPC) using 1,2,4-trichlorobenzene (TCB) as the eluent at 150℃ and monodispersed polystyrene as the standard.

Optical measurements and simulations. Ultraviolet-visible near-infrared (UV-vis-NIR) absorption spectra were recorded with a Perkin-Elmer Lambda 365 UV-Vis spectrophotometer from 300 nm to 1100 nm. The optical simulations were calculated by Fluxim Setfos software.

Atomic force microscopy (AFM) measurements. AFM measurements were performed with a Nano Wizard 4 atomic force microscopy (JPK Inc. Germany) in Qi mode to observe the films surface morphologies of the Glass/PEDOT:PSS/Active layer.

Transmission electron microscopy (TEM) measurements. TEM measurements were carried out using a 200 kV (JEOL ARM-200F). Samples for TEM were prepared on a Cu mesh grid.

Transient photocurrent (TPC) measurements. Relevant solar cells were excited with a 405 nm laser diode. The transient photocurrent response of the devices at short circuit condition to a 200 μs square pulse from the LED with no background illumination. The current traces were recorded on a Tektronix DPO3034 digital oscilloscope by measuring the voltage drop over a 5-ohm sensor resistor in series with the solar cell. DC voltage was applied to the solar cell with an MRF544 bipolar junction transistor in a common collector amplifier configuration.

Transient photovoltage (TPV) measurements. For TPV measurements, devices were directly connected to an oscilloscope in open-circuit conditions (1MΩ). A small optical perturbation was applied using a 405 nm laser-diode which was adjusted in light intensity to produce a voltage perturbation of $\Delta Vo < 10$ mV $\ll Voc$. The amounts of charges generated by the pulse was obtained by integrating a photocurrent measurement (50 Ω) without bias light.

Photo-induced charge carrier extraction by linearly increasing the voltage (photo-CELIV) measurements. In photo-CELIV measurements, the devices were illuminated with a 405 nm laser diode. Current transients were recorded across the internal 50-ohm resistor of our oscilloscope. Here, a fast electricity switch was used to isolate the device in order to prevent carrier extraction or sweep out. After the variable delay time, the switch connected the device to a function generator. It applied a linear extraction ramp, which was 40 μs long and 2.0 V high. Moreover, it started with an offset matching the V_{oc} of the device for each delay time. To determine the mobility in the devices, photo-CELIV curves were measured using different experimental conditions, differing in delay time and applied voltage.

In situ photoluminescence (in-situ PL) spectroscopy. The in-situ PL measurements were conducted by QE65PRO spectrometer (Ocean Optics, USA) for investigating the film formation and thermal annealing treatments. In addition, the thermal degraded PL data and emission of relevant films were collected using a Zolix Flex One Spectrometer. The PL excitation wavelength was set to 532 nm.

In situ Ultraviolet-visible (in-situ UV) absorption spectra. For in-situ absorption spectra, an HL-2000 from Ocean Optics was used as the VIS-NIR light source, and a QE65PRO with high-performance spectrometer from Ocean Optics was used as a detector. The characterization was through the transmission mode. The minimum integration time was 8 ms with automatically recorded spectra every 50 ms.

Surface energy tests. Contact angle measurements were performed on a contact angle measurement system (Attention Theta Lite) using water or ethylene glycol as the wetting liquid, and surface energy values, calculated with the OWRK model, for the different samples.

Photo Stability test. The fabrication process of devices for stability testing is consistent with what is mentioned above. The photo-stability of devices was performed in an N_2-filled glovebox and illuminated by an array of white LEDs with an intensity equivalent to one sun, calibrated by the light meter (TES-1332A, TES Electrical Electronic Corp.).

2. Figure and Tables

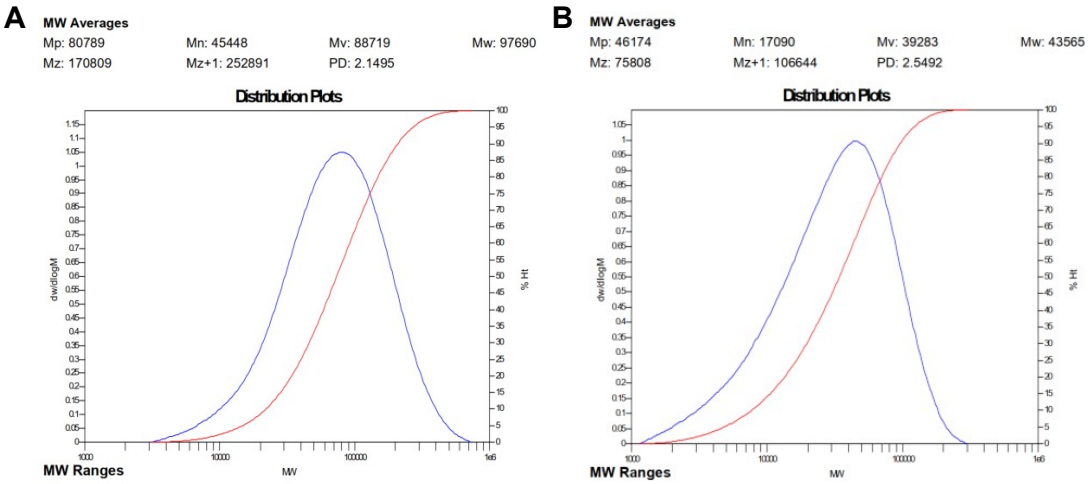

Figure S1. The molecular weights of two PM6 batches ((A) PM6 and (B) $PM6_L$) determined by high-temperature gel permeation chromatography with polystyrene standards.

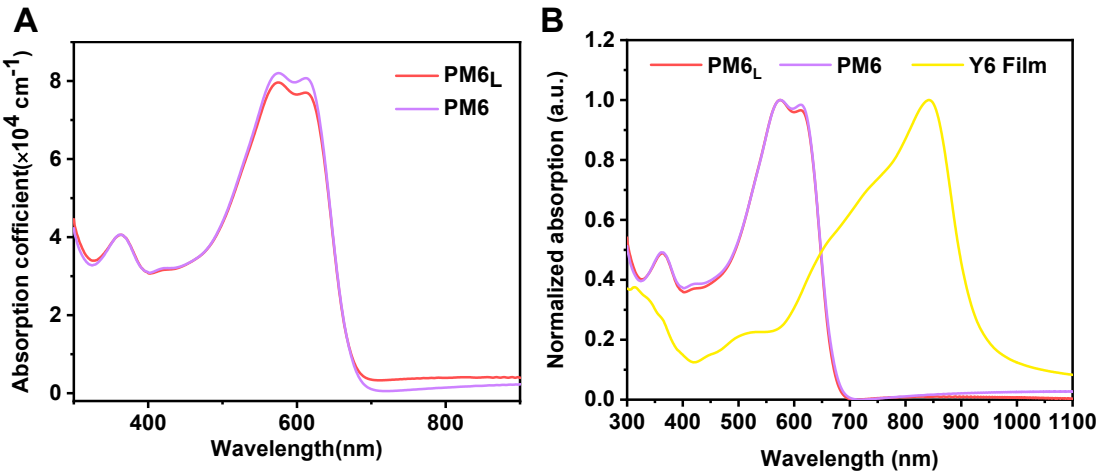

Figure S2. (A) Absorption coefficients of the investigated PM6 and $PM6_L$ donors. (B) Normalized ultraviolet-visible absorption spectra of the investigated materials.

Table S1. Summary of physical properties of the investigated photovoltaic materials.

Materials	M_n[a] (kg mol^{-1})	PDI[a]	Film λ_{max}[b] (nm)	Film λ_{onset}[b] (nm)	E_g^{opt}, [c] (eV)
PM6	45.4	2.15	576	676	1.832
$PM6_L$	17.1	2.55	576	680	1.824
Y6	--	--	842	934	1.328

[a]Measured by GPC technology. [b]Cast from chloroform solution. [c]Bandgap estimated from the onset wavelength (λ_{edge}) of the optical absorption: $E_g^{opt} = 1240/\lambda_{edge}$.

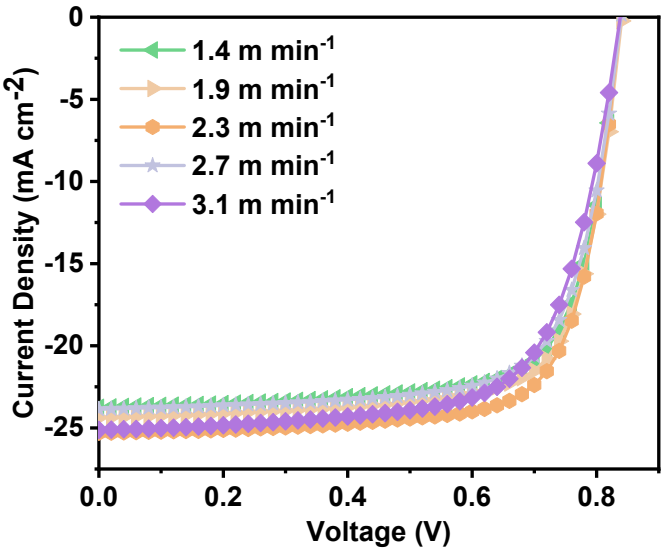

Figure S3. *J-V* curves of the PM6:Y6 devices with different blade-coating speeds measured under one sun illumination.

Table S2. Photovoltaic parameters of the PM6:Y6 devices with different blade-coating speeds, measured under one sun illumination.

Speed [m min^{-1}]	Thickness [nm]	V_{oc} [V]	J_{sc} [mA cm^{-2}]	FF [%]	PCE (Avg.[a]) [%]
1.4	60	0.839	23.74	73.34	14.61 (14.49±0.10)
1.9	87	0.841	24.36	73.57	15.07 (14.95±0.08)
2.3	115	0.838	25.30	73.94	15.67 (15.54±0.08)
2.7	134	0.839	25.34	72.02	15.31 (15.18±0.10)
3.1	150	0.838	25.12	68.98	14.52 (14.37±0.12)

[a] The values in bracket are the average PCE obtained from eight devices.

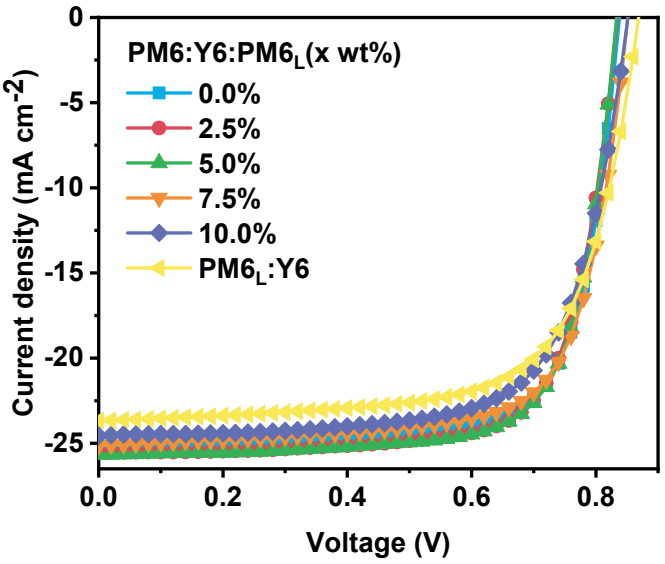

Figure S4. *J-V* curves of the PM6:Y6 devices doped with different $PM6_L$ concentrations, fabricated at a coating speed of 2.3 m min^{-1} and measured under one sun illumination.

Table S3. Photovoltaic parameters of the PM6:Y6 devices doped with different $PM6_L$ concentrations, fabricated at a coating speed of 2.3 m min^{-1}. All wt% in this work are relative to the amount of the host donor PM6 and acceptor Y6.

$PM6_L$ [x wt%]	Thickness [nm]	V_{oc} [V]	J_{sc} [mA cm^{-2}]	FF [%]	PCE (Avg.[a]) [%]
0.0%	115	0.838	25.30	73.94	15.67 (15.54±0.08)
2.5%	106	0.834	25.57	73.90	15.77 (15.66±0.10)
5.0%	109	0.833	25.67	74.04	15.84 (15.73±0.09)
7.5%	101	0.851	25.13	72.07	15.41 (15.23±0.13)
10.0%	98	0.851	24.56	69.69	14.58 (14.44±0.10)
$PM6_L$:Y6	111	0.869	23.67	68.35	14.05 (13.92±0.09)

[a] The values in bracket are the average PCE obtained from eight devices.

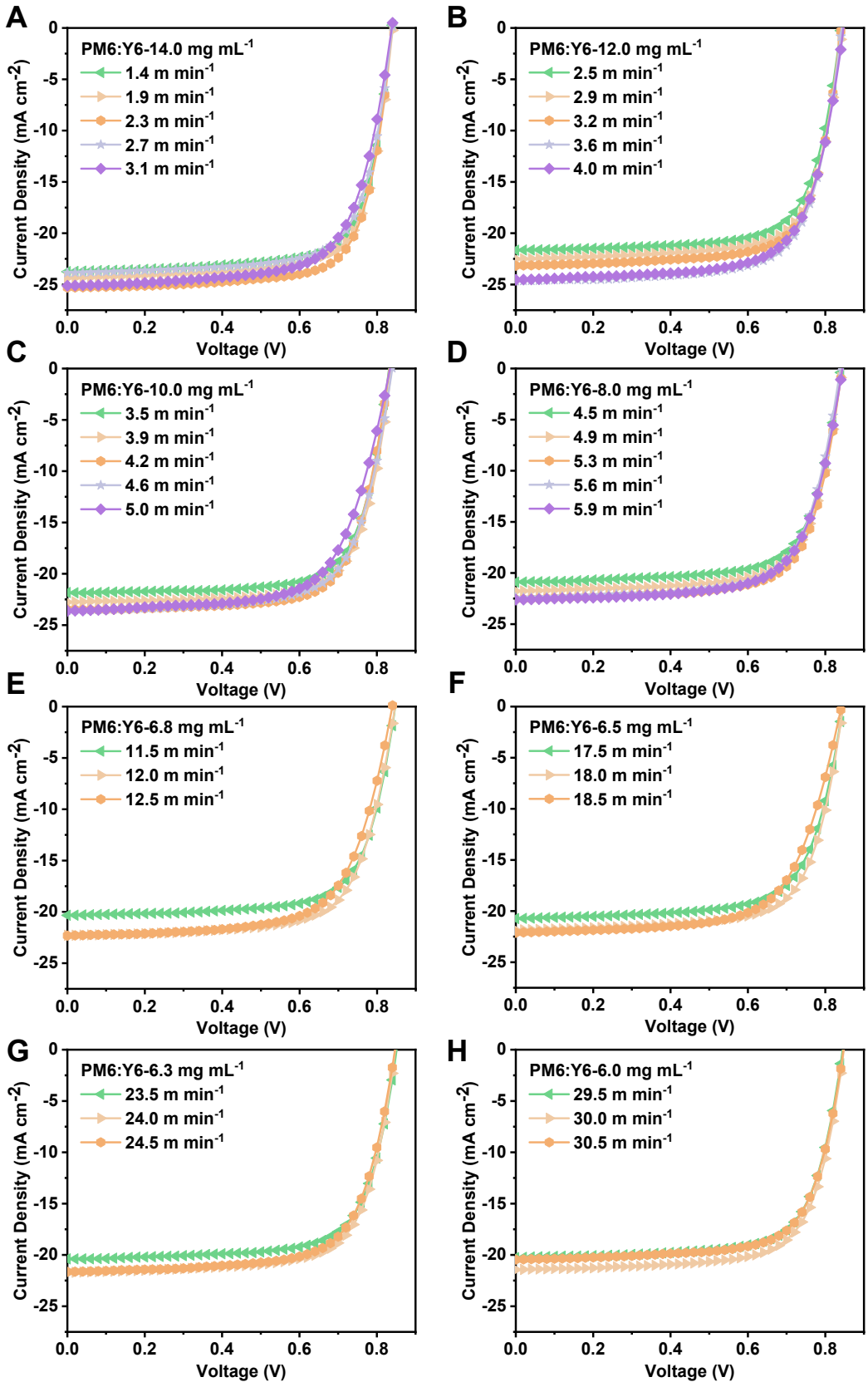

Figure S5. *J-V* curves of the PM6:Y6 devices with different solution concentrations (14.0, 12.0, 10.0, 8.0, 6.8, 6.5, 6.3 and 6.0 mg mL^{-1}, respectively), fabricated at different blade-coating speeds measured under one sun illumination.

Table S4. Photovoltaic parameters of the PM6:Y6 devices fabricated at different blade-coating speeds.

Concentration [mg mL^{-1}]	Speed [m min^{-1}]	Thickness [nm]	V_{oc} [V]	J_{sc} [mA cm^{-2}]	FF [%]	PCE (Avg.[a]) [%]
14.0	1.4	60	0.839	23.74	73.34	14.61 (14.49±0.10)
	1.9	87	0.841	24.36	73.57	15.07 (14.95±0.08)
	2.3	115	0.838	25.30	73.94	15.67 (15.54±0.08)
	2.7	134	0.839	25.34	72.02	15.31 (15.18±0.10)
	3.1	150	0.838	25.12	68.98	14.52 (14.37±0.12)
12.0	2.5	64	0.841	23.04	72.17	13.98 (13.85±0.11)
	2.9	73	0.843	23.86	72.59	14.60 (14.48±0.10)
	3.2	99	0.841	24.51	72.75	15.00 (14.92±0.06)
	3.6	115	0.842	24.67	71.51	14.85 (14.79±0.05)
	4.0	132	0.847	24.54	70.01	14.55 (14.42±0.11)
10.0	3.5	76	0.832	21.83	73.01	13.26 (13.16±0.07)
	3.9	98	0.838	22.76	72.49	13.83 (13.68±0.12)
	4.2	110	0.833	23.48	72.15	14.11 (13.95±0.09)
	4.6	125	0.840	23.56	69.95	13.84 (13.70±0.10)
	5.0	139	0.834	23.62	66.76	13.15 (13.05±0.09)
8.0	4.5	65	0.841	20.89	71.54	12.57 (12.42±0.13)
	4.9	87	0.843	21.77	71.46	13.11 (12.93±0.14)
	5.3	106	0.843	22.57	71.36	13.58 (13.45±0.10)
	5.6	129	0.839	22.43	70.07	13.19 (13.09±0.08)
	5.9	146	0.844	22.61	69.56	13.28 (13.17±0.10)

6.8	11.5	98	0.847	20.33	71.63	12.33 (12.20±0.10)
	12	109	0.846	22.29	70.41	13.28 (13.19±0.08)
	12.5	123	0.839	22.32	67.31	12.61 (12.50±0.08)
6.5	17.5	76	0.846	20.73	70.07	12.28 (12.18±0.07)
	18	97	0.846	21.86	70.93	13.11 (12.98±0.09)
	18.5	113	0.842	22.12	66.58	12.40 (12.26±0.10)
6.3	23.5	84	0.851	20.39	71.55	12.42 (12.27±0.13)
	24	108	0.848	21.72	71.60	13.18 (13.04±0.10)
	24.5	134	0.847	21.65	69.93	12.82 (12.70±0.10)
6.0	29.5	95	0.845	20.26	71.84	12.30 (12.17±0.12)
	30	112	0.848	21.44	71.42	12.98 (12.88±0.09)
	30.5	136	0.847	21.53	71.22	12.34 (12.24±0.08)

[a] The values in bracket are the average PCE obtained from eight devices.

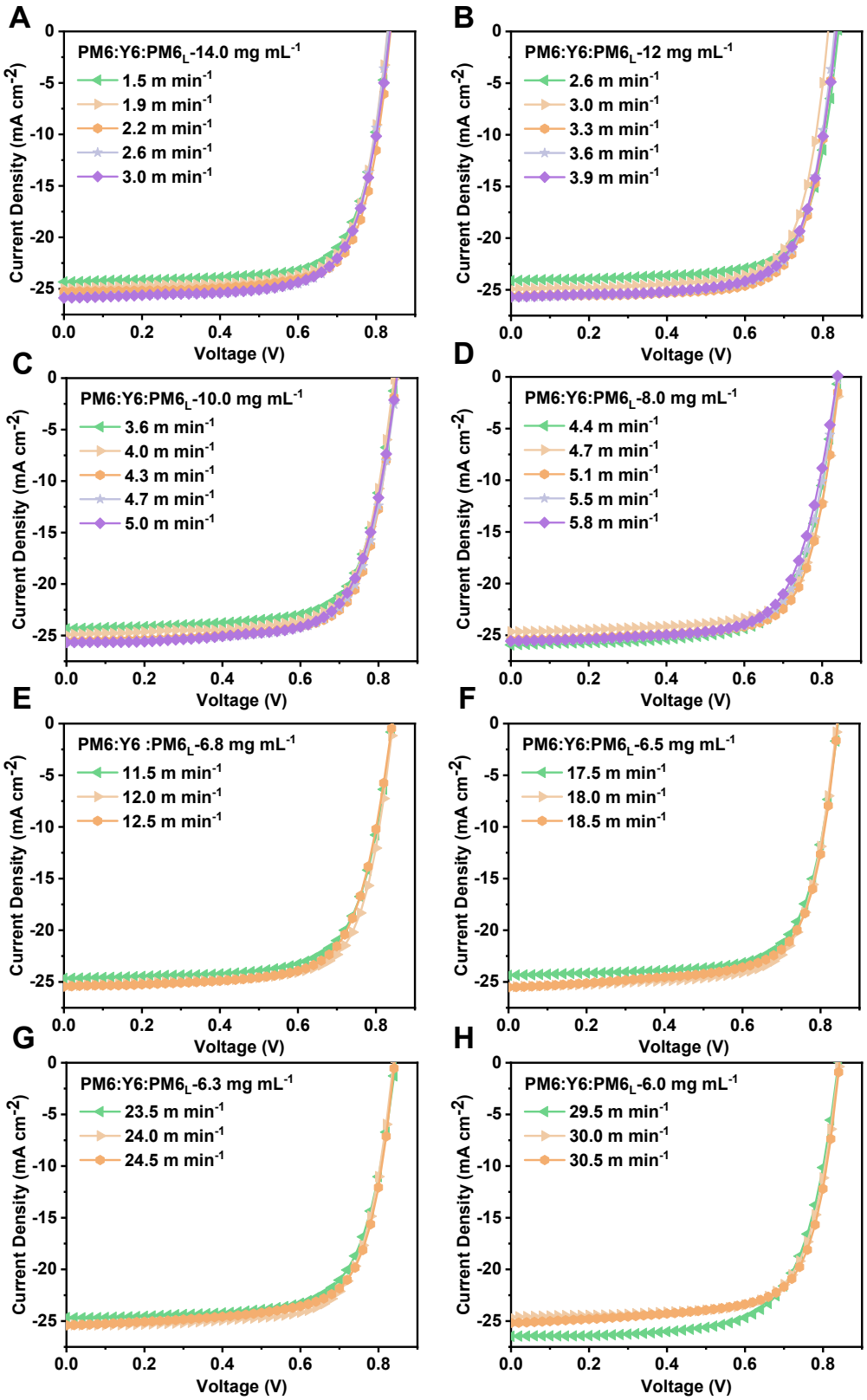

Figure S6. *J-V* curves of the 5 wt% $PM6_L$-doped PM6:Y6 devices with different solution concentrations (14.0, 12.0, 10.0, 8.0, 6.8, 6.5, 6.3 and 6.0 mg mL^{-1}, respectively), fabricated at different blade-coating speeds measured under one sun illumination.

Table S5. Photovoltaic parameters of the PM6:Y6 (5 wt% $PM6_L$) devices with different solution concentrations, fabricated at different blade-coating speeds.

Concentration [mg mL^{-1}]	Speed [m min^{-1}]	Thickness [nm]	V_{oc} [V]	J_{sc} [mA cm^{-2}]	FF [%]	PCE (Avg.[a]) [%]
14.0	1.5	76	0.835	24.34	72.83	14.80 (14.66±0.13)
	1.9	95	0.829	25.02	73.42	15.23 (15.05±0.14)
	2.2	112	0.837	25.74	74.08	15.96 (15.80±0.13)
	2.6	136	0.830	25.76	73.08	15.63 (15.44±0.16)
	3.0	149	0.835	25.88	71.81	15.52 (15.41±0.08)
12.0	2.6	65	0.840	24.11	73.77	14.94 (14.82±0.10)
	3.0	84	0.833	24.93	74.05	15.38 (15.23±0.14)
	3.3	106	0.833	25.62	74.17	15.83 (15.74±0.07)
	3.6	125	0.830	25.70	73.28	15.63 (15.43±0.16)
	3.9	141	0.835	25.68	71.95	15.43 (15.31±0.08)
10.0	3.6	76	0.844	24.34	71.92	14.77 (14.63±0.10)
	4.0	97	0.840	24.91	72.26	15.12 (14.98±0.12)
	4.3	111	0.845	25.55	73.01	15.76 (15.57±0.17)
	4.7	136	0.848	25.61	71.95	15.63 (15.50±0.12)
	5.0	152	0.847	25.67	70.85	15.40 (15.28±0.10)
8.0	4.4	76	0.842	23.87	70.99	14.27 (14.14±0.09)
	4.7	89	0.845	24.66	72.88	15.19 (15.02±0.13)
	5.1	108	0.844	25.46	73.16	15.72 (15.60±0.10)
	5.5	125	0.841	25.51	71.24	15.28 (15.09±0.16)
	5.8	142	0.840	25.57	69.96	15.03 (14.95±0.05)

6.8	11.5	86	0.842	24.67	71.11	14.77 (14.72±0.01)
	12.0	105	0.843	25.39	73.07	15.64 (15.50±0.10)
	12.5	132	0.842	25.44	70.99	15.21 (15.02±0.14)
6.5	17.5	79	0.845	24.36	72.36	14.89 (14.74±0.10)
	18.0	98	0.842	25.47	73.03	15.66 (15.51±0.12)
	18.5	114	0.844	25.51	71.10	15.31 (15.19±0.08)
6.3	23.5	74	0.844	24.65	71.15	14.80 (14.68±0.10)
	24.0	95	0.838	25.37	72.96	15.51 (15.40±0.08)
	24.5	121	0.841	25.41	71.47	15.27 (15.14±0.11)
6.0	29.5	79	0.840	24.73	69.16	14.37 (14.25±0.10)
	30.0	103	0.841	25.42	72.72	15.55 (15.40±0.13)
	30.5	134	0.842	25.14	71.61	15.16 (15.03±0.10)

[a] The values in bracket are the average PCE obtained from eight devices.

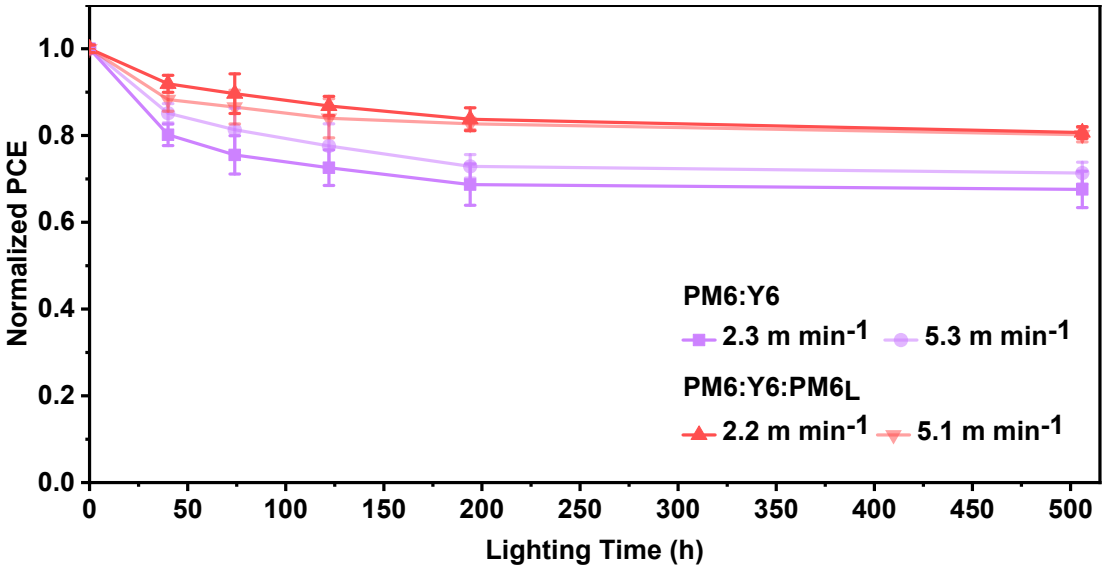

Figure S7. Evolution of the degradation trends of the PM6:Y6 devices without and with $PM6_L$-doping, fabricated at various coating-speeds and measured under one sun illumination. All degradation data are averaged values of at least five solar cells.

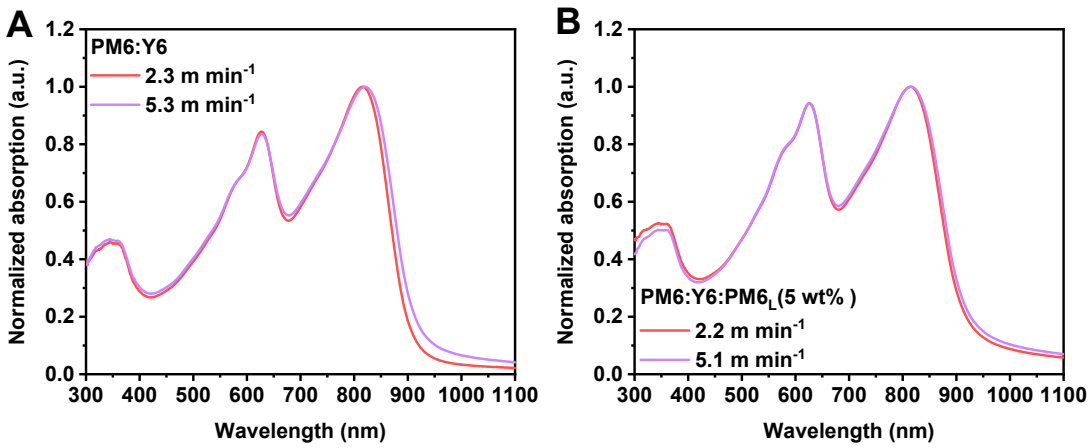

Figure S8. Ultraviolet-visible (UV-Vis) absorption spectra of the PM6:Y6 blends (A) without and (B) with 5 wt% $PM6_L$ doping, fabricated at low and high coating-speeds.

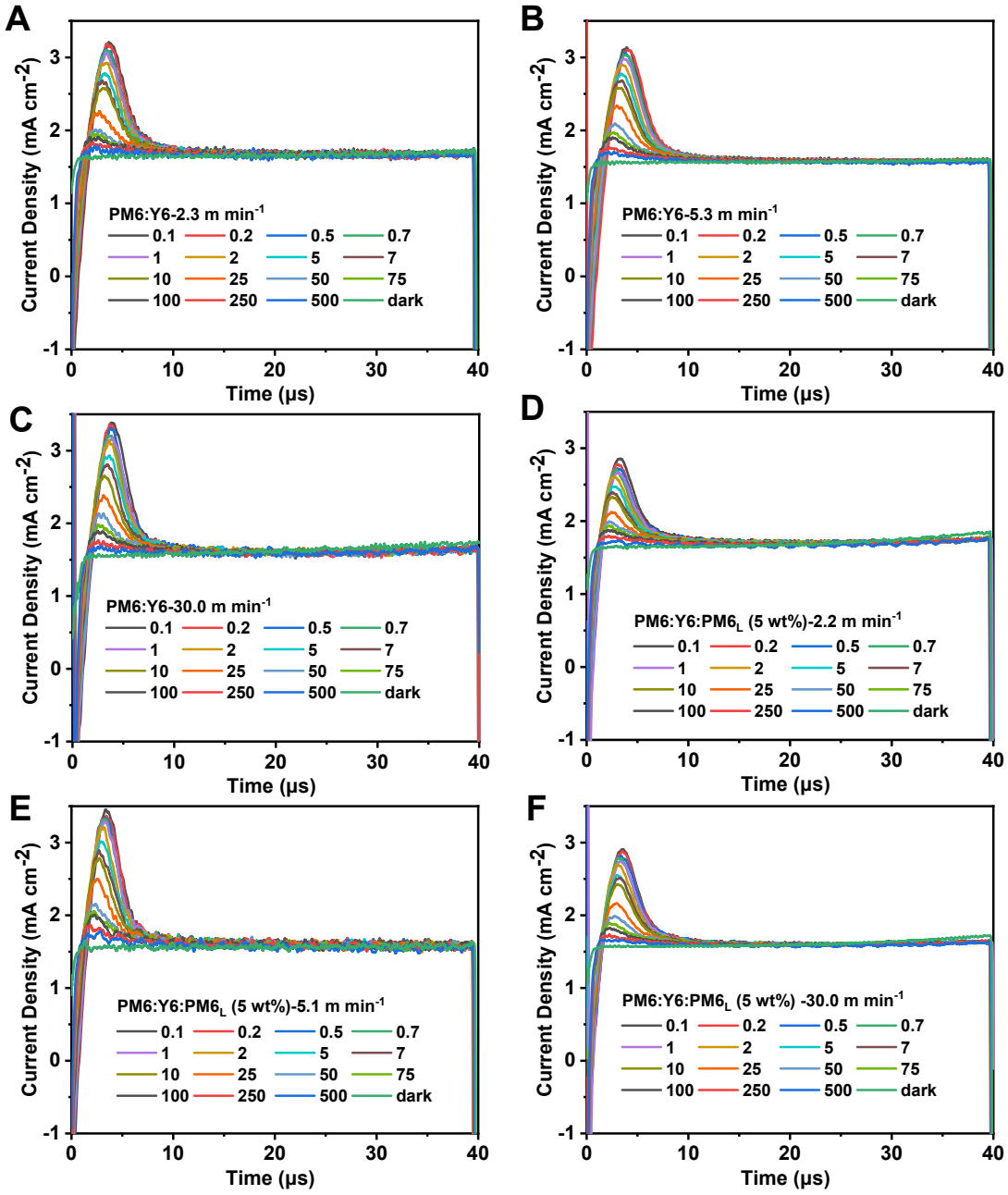

Figure S9. The Photo-CELIV traces of PM6:Y6 devices fabricated at (A) 2.3 m min^{-1}, (B) 5.3 m min^{-1} and (C) 30.0 m min^{-1} and of $PM6_L$-doped PM6:Y6 devices fabricated at (D) 2.2 m min^{-1}, (E) 5.1 m min^{-1} and (F) 30.0 m min^{-1} for different delay times between the light pulse and the extraction voltage ramp.

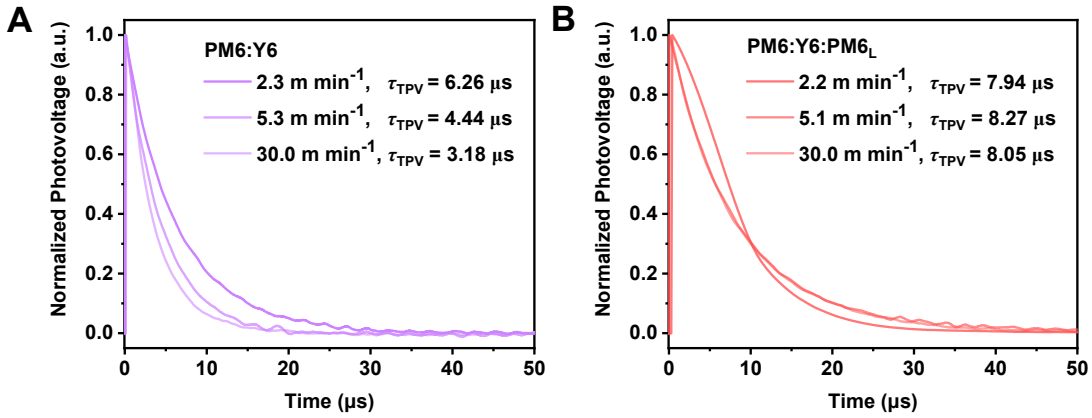

Figure S10. Transient photovoltage (TPV) measurements of the devices (A) without and (B) with $PM6_L$-doping, fabricated at various coating-speeds.

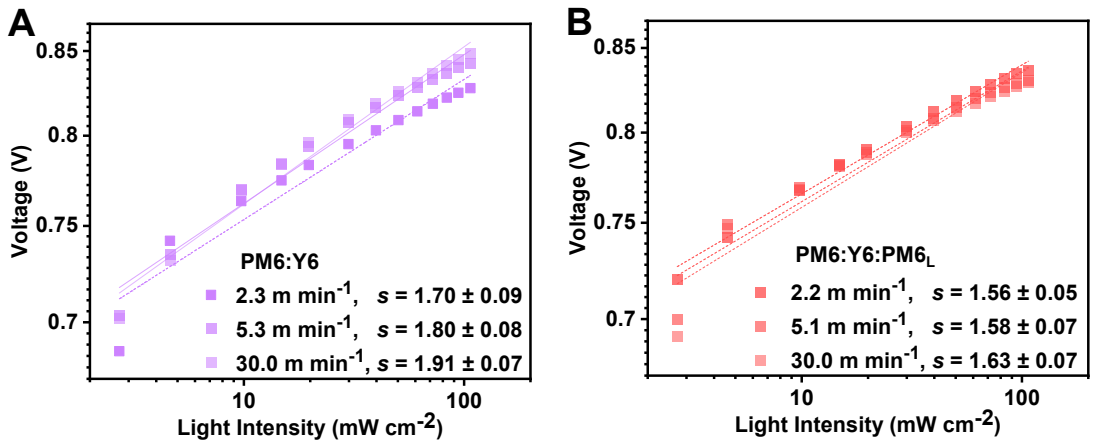

Figure S11. Voltage against the light intensity of the devices (A) without and (B) with $PM6_L$-doping, fabricated at various coating speeds. The V_{oc} and light intensity (I) can be correlated by the expression of $V_{OC} = \frac{E_{gap}}{q} - \frac{kT}{q}\ln[\frac{(1-P)\gamma N_c^2}{PG}]$, where E_{gap} is the energy gap, q is the elementary charge, k is the Boltzman constant, T is the temperature in Kelvin, P is the dissociation probability of the electron-hole pairs into free carriers, γ the recombination constant, N_c is the density of states in the conduction band, and G the generation rate of electron-hole pairs. Following the rules, the formula predicts a slope $S = (kT/q)$ of the V_{oc} versus the natural logarithm of the incident light intensity. This implies that the slope of V_{oc} versus $\ln(I)$ is equal to kT/q for bimolecular recombination. When the additional mechanism of Schockley-Real-Hall (SRH) or trap-assisted recombination is involved, a stronger dependency of V_{oc} on the light intensity is observed, and in this case, the slope of V_{oc} versus $\ln(I)$ is equal to 2 kT/q. The error bar is calculated from five devices. As compared to the doped devices, the slightly stronger dependence of V_{oc} on light intensity implies that carrier dynamics at an open circuit in a BHJ device is slightly governed by a combination of trap-assisted (SRH) type and bimolecular recombination. The use of a doped layer reduces the trap-assisted recombination as seen from the slope values.

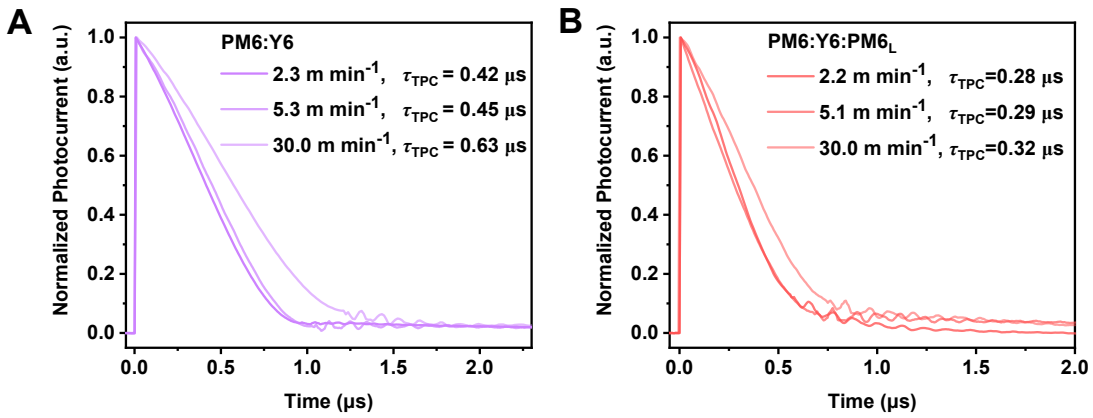

Figure S12. Normalized transient photocurrent (TPC) measurements of the devices (A) without and (B) with $PM6_L$-doping, fabricated at various coating speeds. A 405 nm diode laser turned off at 50 μs is used as the light source to excite the cell, and the transient photocurrent is recorded.

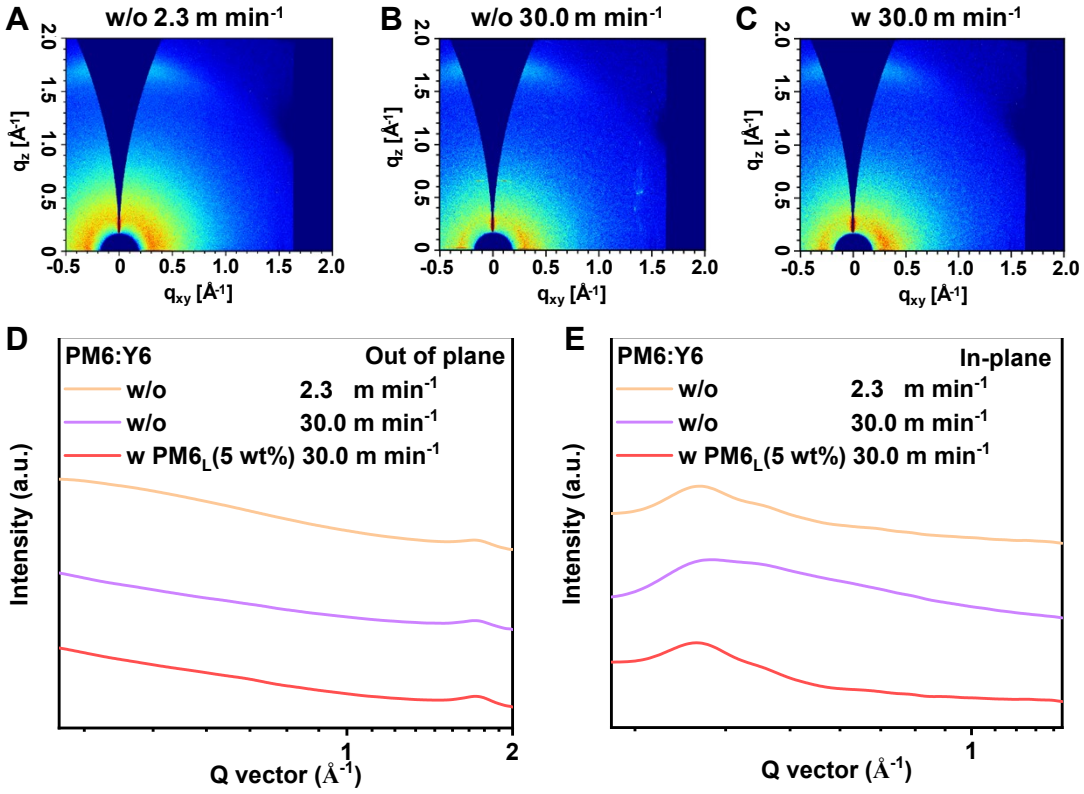

Figure S13. 2D GIWAXS patterns of the fresh (A) PM6:Y6 w/o fabricated at 2.3 m min^{-1}, (B) PM6:Y6 w/o fabricated at 30.0 m min^{-1} and (C) PM6:Y6 w 5 wt% fabricated at 30.0 m min^{-1} films. GIWAXS line cuts of the corresponding blend films with respect to the (D) out-of-plane and (E) in-plane directions.

Table S6. Investigations of the morphology parameters extracted from the GIWAXS measurements of the PM6:Y6 blend films fabricated at w/o 2.3 m min^{-1}, w/o 30.0 m min^{-1}, w 30.0 m min^{-1}.

PM6:Y6	In plane (100)		Out of plane (010)			
	q (Å^{-1})	*d* (Å)	*q* (Å^{-1})	*d* (Å)	FWHM (Å^{-1})	CCL (Å)
w/o 2.3 m min^{-1}	0.298	21.07	1.707	3.679	0.265	23.70
w/o 30.0 m min^{-1}	0.311	20.19	1.709	3.674	0.442	14.20
w 30.0 m min^{-1}	0.296	21.22	1.710	3.673	0.281	22.35

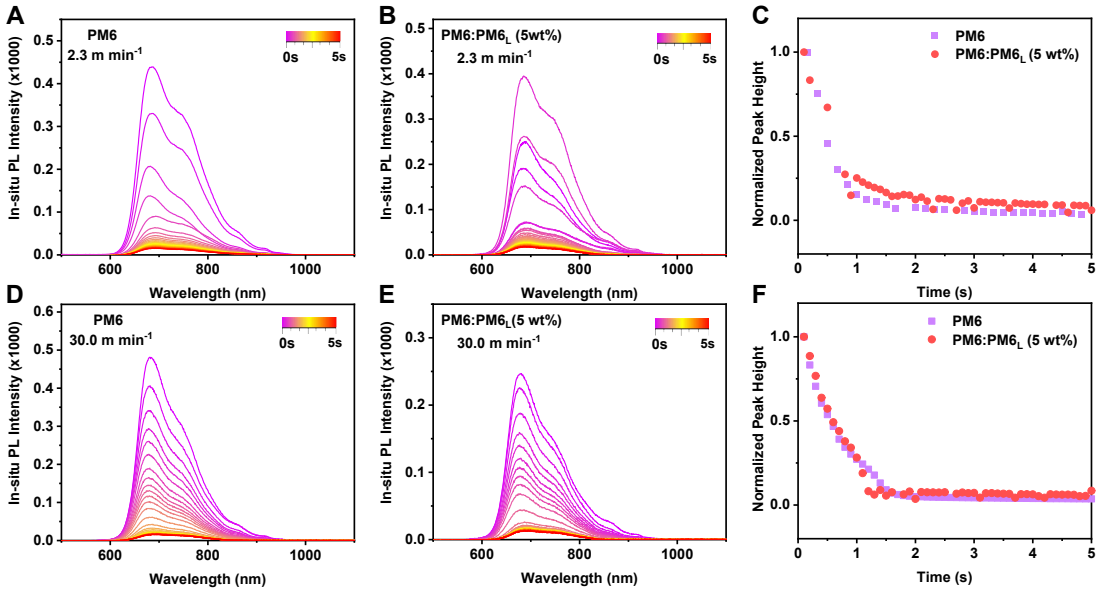

Figure S14. (A and B) Evolution of *in-situ* PL during the film formation processes of the (A) dopant-free and (B) $PM6_L$-doped PM6 layers fabricated at a blade coating speed of 2.3 m min^{-1}. (C) The corresponding normalized peak height of the dopant-free and $PM6_L$-doped PM6 layers fabricated at a coating speed of 2.3 m min^{-1}, plotted from 0 to 5.0 s. (D and E) Evolution of *in-situ* PL during the film formation processes of the (D) dopant-free and (E) $PM6_L$-doped PM6 layers fabricated at a coating speed of 30.0 m min^{-1}. (F) The corresponding normalized peak height of the dopant-free and $PM6_L$-doped PM6 layers fabricated at a coating speed of 30.0 m min^{-1}, plotted from 0 to 5.0 s. The PL intensity intensities of the dopant-free and $PM6_L$-doped PM6 gradually reduced from 0 to 5 s. It is because during the film formation, the rapid removal of solvent due to heating of the baseplate concentrated the D:A mixture and rapidly drove the wetting deposition to the layer-thinning transition.

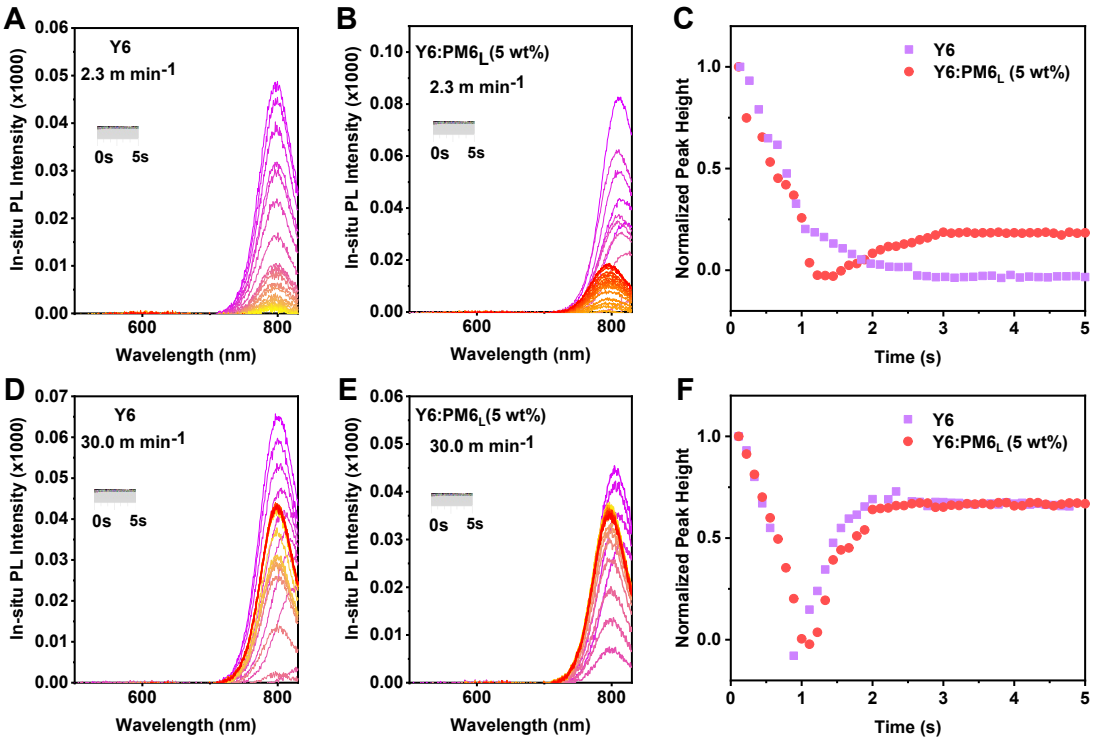

Figure S15. (A and B) Evolution of *in-situ* PL during the film formation processes of the (A) dopant-free and (B) $PM6_L$-doped Y6 layers fabricated at a blade coating speed of 2.3 m min^{-1}. (C) The corresponding normalized peak height of the dopant-free and $PM6_L$-doped Y6 layers fabricated at a coating speed of 2.3 m min^{-1}, plotted from 0 to 5.0 s. (D and E) Evolution of *in-situ* PL during the film formation processes of the (D) dopant-free and (E) $PM6_L$-doped Y6 layers fabricated at a coating speed of 30.0 m min^{-1}. (F) The corresponding normalized peak height of the dopant-free and $PM6_L$-doped Y6 layers fabricated at a coating speed of 30.0 m min^{-1}, plotted from 0 to 5.0 s.

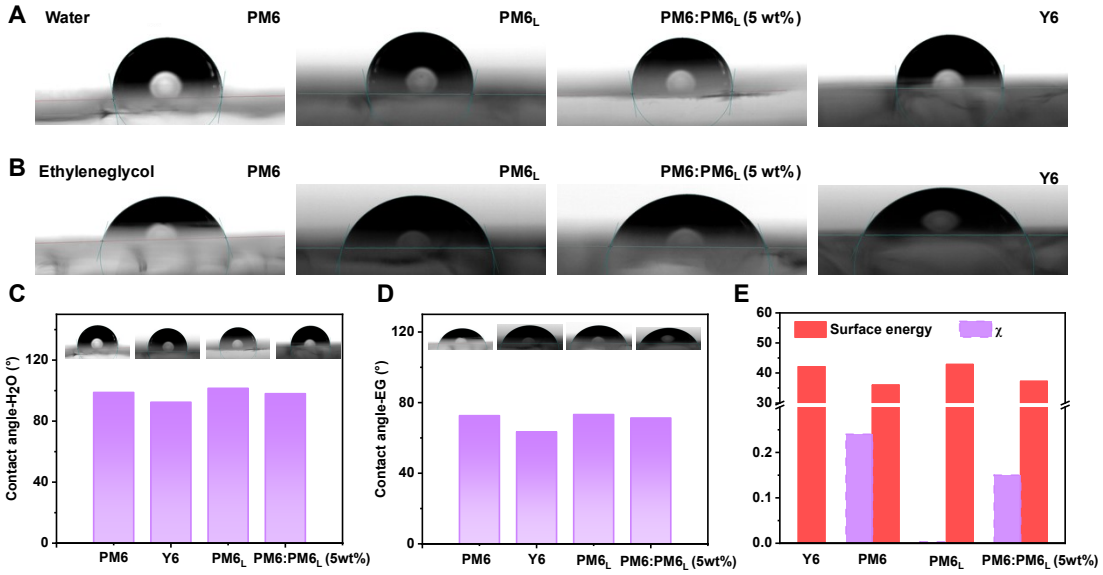

Figure S16. Surface energy measurements ((A) water and (B) ethylene glycol) of the investigated photovoltaic materials and the PM6:$PM6_L$ mixture. Distilled water (C) and ethylene glycol (D) contact angles measured on the surfaces of the neat films and the $PM6_L$-doped PM6 film. (E) The surface energy of the corresponding films and χ values of relevant BHJ systems. In detail, we used water and ethylene glycol to conduct the surface energy tests of these three photovoltaic materials and the PM6:$PM6_L$ (5 wt%) mixture. As summarized in **Table S7**, the related surface energy values are 35.96 mN m^{-1} for PM6, 42.04 mN m^{-1} for Y6, 42.80 mN m^{-1} for $PM6_L$, and 37.20 mN m^{-1} for PM6:$PM6_L$ (5 wt%) mixture, respectively. The Flory-Huggins interaction parameter (χ) values were calculated to be 0.24 *K* for PM6:Y6, 0.003 *K* for $PM6_L$:Y6, 0.30 *K* for PM6:$PM6_L$, respectively, as depicted in **Figure S16E**. A high χ value of 0.24 *K* suggests the severe phase separation in the PM6:Y6 active layer fabricated at a high coating speed owing to the rapid solvent evaporation, which was demonstrated by the AFM measurement (**Figure 2A**). The surface energy results further illustrate $PM6_L$:Y6 with a χ of 0.003 *K* possesses stronger intermolecular interactions as compared to PM6 and $PM6_L$ (a χ of 0.30 *K*). The PM6:$PM6_L$:Y6 shows a lower χ value of 0.15 K in comparison to PM6:Y6, indicating that a small amount of $PM6_L$ can effectively improve the molecular compatibility of PM6 and Y6 materials. This result is also evident that both phase separation and material aggregation occurred more slowly with a decrease in solvent concentration in comparison to the dopant-free PM6:Y6 system, supported by the in-situ spectroscopy measurements (**Figure 3**).

Table S7. The surface energy of the investigated photovoltaic materials and the PM6：$PM6_L$ (5 wt %) mixture.

Materials	Contact		Surface energy [mN m^{-1}]	Relative χ	
	Water	Ethylene glycol		with Y6	With $PM6_L$
PM6	98.8 (98.8±0.10)	72.6 (72.6±0.05)	35.96 (35.96±0.06）	0.24*K*	0.30*K*
Y6	92.4 (92.4±0.05)	63.4 (63.4±0.10)	42.04 (42.04±0.07）	/	0.003*K*
$PM6_L$	101.5 (101.5±0.0)	73.25 (73.25±0.05)	42.80 (42.80±0.08）	0.003 *K*	/
PM6 (5 wt% $PM6_L$)	98.0 (98.0±0.05)	71.3 (71.3±0.05)	37.20 (37.2±0.08）	0.15*K*	/

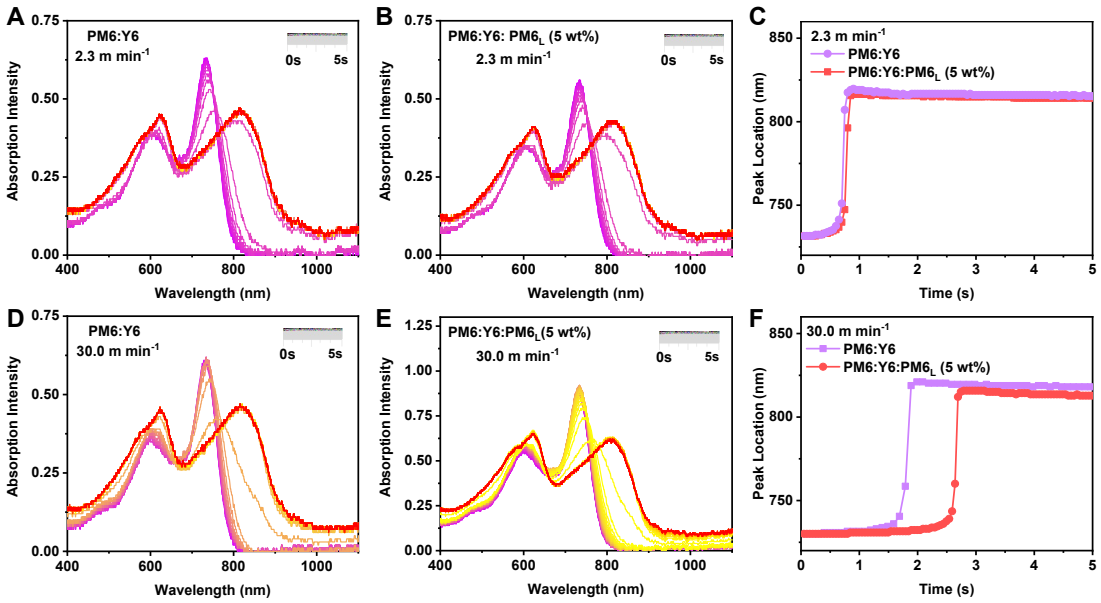

Figure S17. Evolution of in-situ UV during the film formation processes of the (A) dopant-free and (B) $PM6_L$-doped active layers fabricated at a coating speed of 2.3 m min^{-1}. (C) The corresponding peak location of the dopant-free and $PM6_L$-doped active layers fabricated at a coating speed of 2.3 m min^{-1}, plotted from 0 to 5.0 s. Evolution of in-situ UV during the film formation processes of the (D) dopant-free and (E) $PM6_L$-doped active layers fabricated at a coating speed of 30.0 m min^{-1}. (F) The corresponding peak location of the dopant-free and $PM6_L$-doped active layers fabricated at a coating speed of 30.0 m min^{-1}, plotted from 0 to 5.0 s.

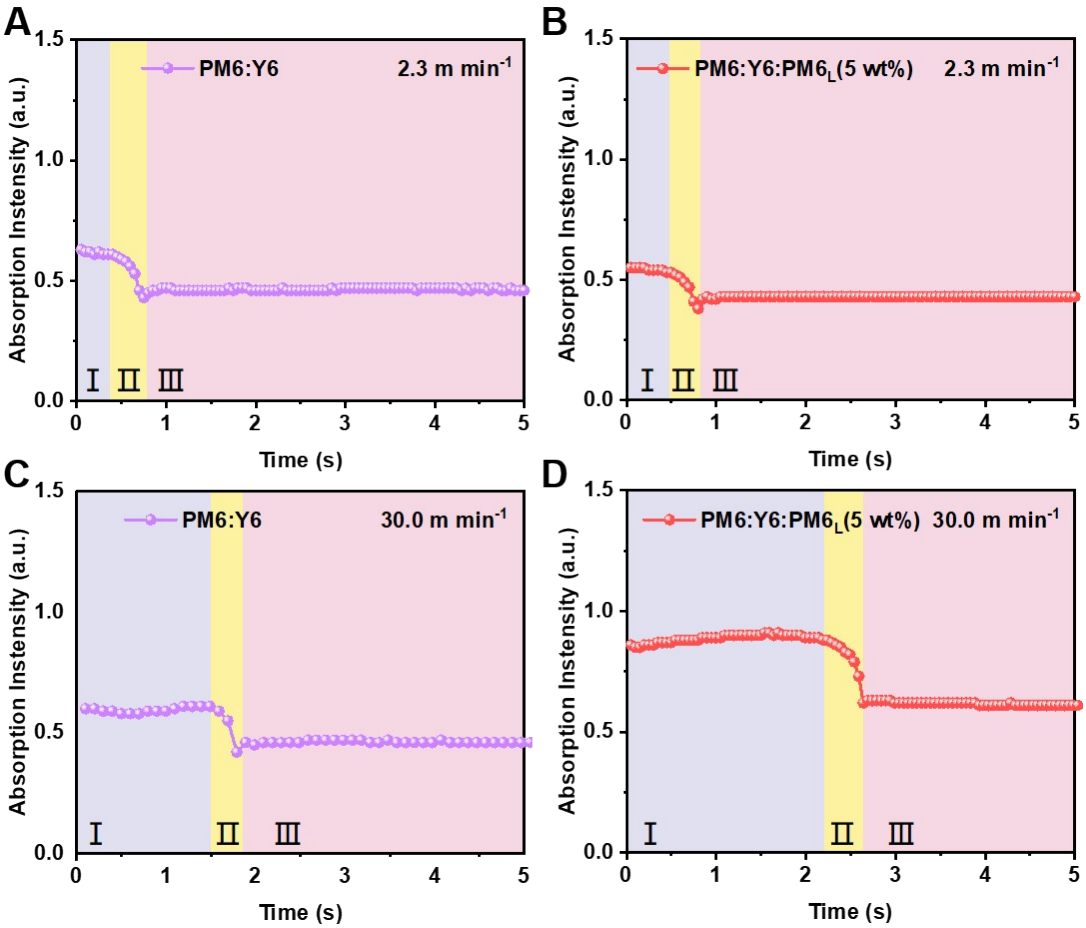

Figure S18. Corresponding changes in the integrated *in-situ* absorption intensities for dopant-free (A and C) and $PM6_L$-doped (B and D) fabricated at the blade-coating speeds of 2.3 and 30.0 m min^{-1}, respectively. Solvent evaporation stage (light grey area) (I) liquid-solid transition (light yellow area) (II), and film formation stage (light pink area) (III).

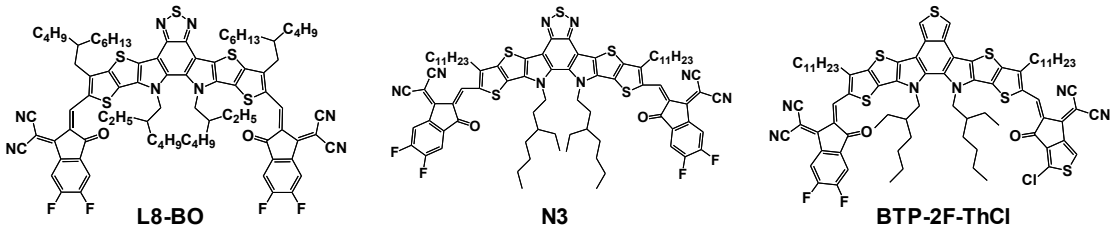

Figure S19. The chemical structures of the investigated small molecule acceptors, including L8-BO, N3 and BTP-2F-ThCl.

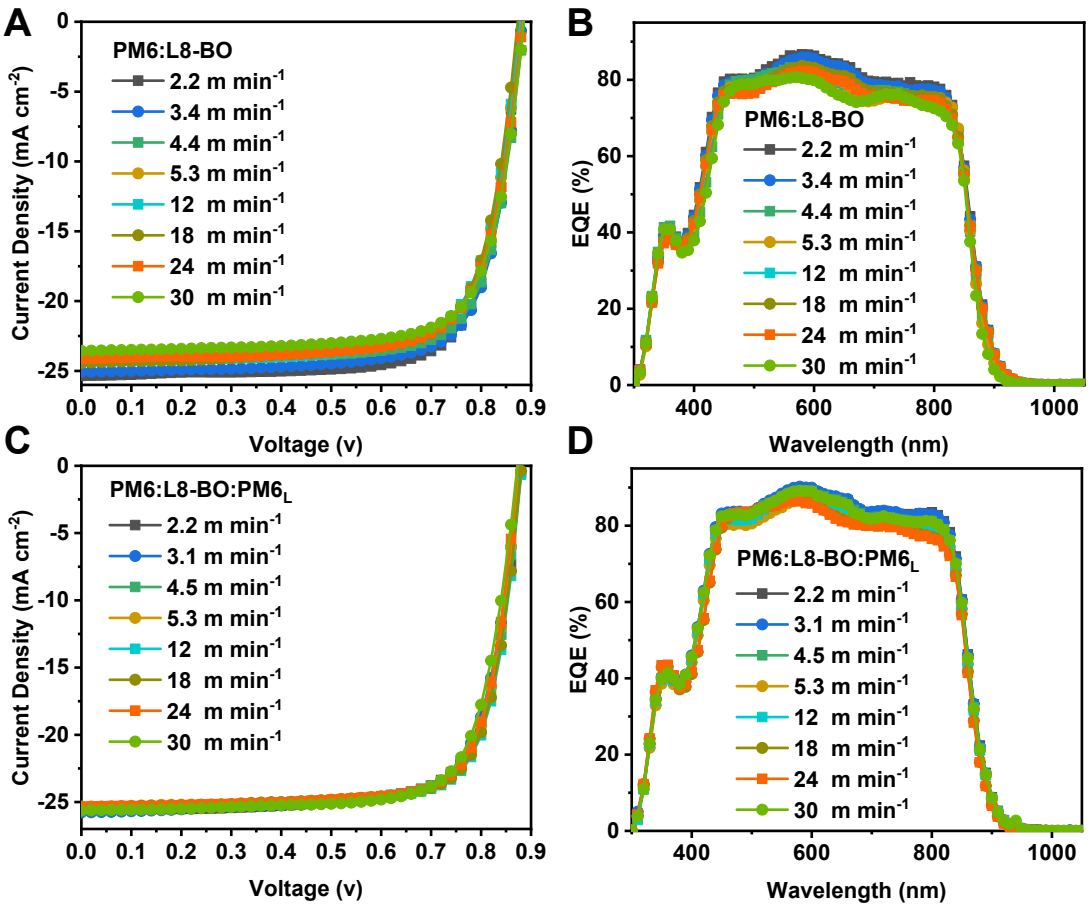

Figure S20. *J–V* characteristics of (A) dopant-free and (C) $PM6_L$-doped PM6:L8-BO systems OSCs with maximum PCE on different solution concentrations under constant incident light intensity (AM 1.5 G, 100 mW cm^{-2}), and the corresponding EQE spectra for (B) dopant-free and (D) $PM6_L$-doped devices.

Table S8. Photovoltaic parameters of PM6:L8-BO (5 wt% $PM6_L$) devices with different blade-coating speeds.

Active layer	Concentration/Speed [mg/mL]/ [m/min]	Thickness [nm]	V_{oc} [V]	J_{sc} [mA cm^{-2}]	$J_{sc\ cal.}$[a] [mA cm^{-2}]	FF [%]	PCE[b] [%]
PM6: L8-BO	14.0/ 2.2	103	0.877	25.35	24.67	77.02	17.13 (16.98±0.10)
	12.0/ 3.4	116	0.881	25.05	24.31	75.14	16.59 (16.45±0.12)
	10.0/ 4.4	105	0.885	24.35	23.68	75.35	16.24 (16.14±0.08)
	8.0/ 5.3	94	0.879	24.18	23.50	74.04	15.74 (15.62±0.09)
	6.8/ 12.0	114	0.878	24.29	23.70	73.53	15.69 (15.55±0.11)
	6.5/ 18.0	110	0.873	24.42	23.87	73.98	15.78 (15.58±0.15)
	6.3/ 24.0	101	0.883	24.13	23.52	73.93	15.75 (15.60±0.09)
	6.0/ 30.0	97	0.885	23.56	22.97	74.75	15.59 (15.46±0.10)
PM6: L8-BO: 5 wt% $PM6_L$	14.0/ 2.2	112	0.881	25.50	24.66	75.05	16.87 (16.69±0.16)
	12.0/ 3.1	106	0.876	25.77	24.75	74.84	16.90 (16.80±0.06)
	10.0/ 4.5	108	0.877	25.43	24.64	76.20	16.99 (16.87±0.08)
	8.0/ 5.3	114	0.875	25.33	24.41	77.24	17.12 (16.98±0.09)
	6.8/ 12.0	109	0.881	25.51	24.62	76.75	17.26 (17.12±0.10)
	6.5/ 18.0	96	0.881	25.39	24.58	76.85	17.19 (17.02±0.14)
	6.3/ 24.0	105	0.873	25.34	24.49	76.86	17.01 (16.90±0.08)
	6.0/ 30.0	107	0.873	25.63	24.70	75.26	16.83 (16.68±0.12)

[a] $J_{sc\ cal}$ represents the integrated current density obtained from EQE spectra. [b] The values in the bracket are the average PCE obtained from eight devices.

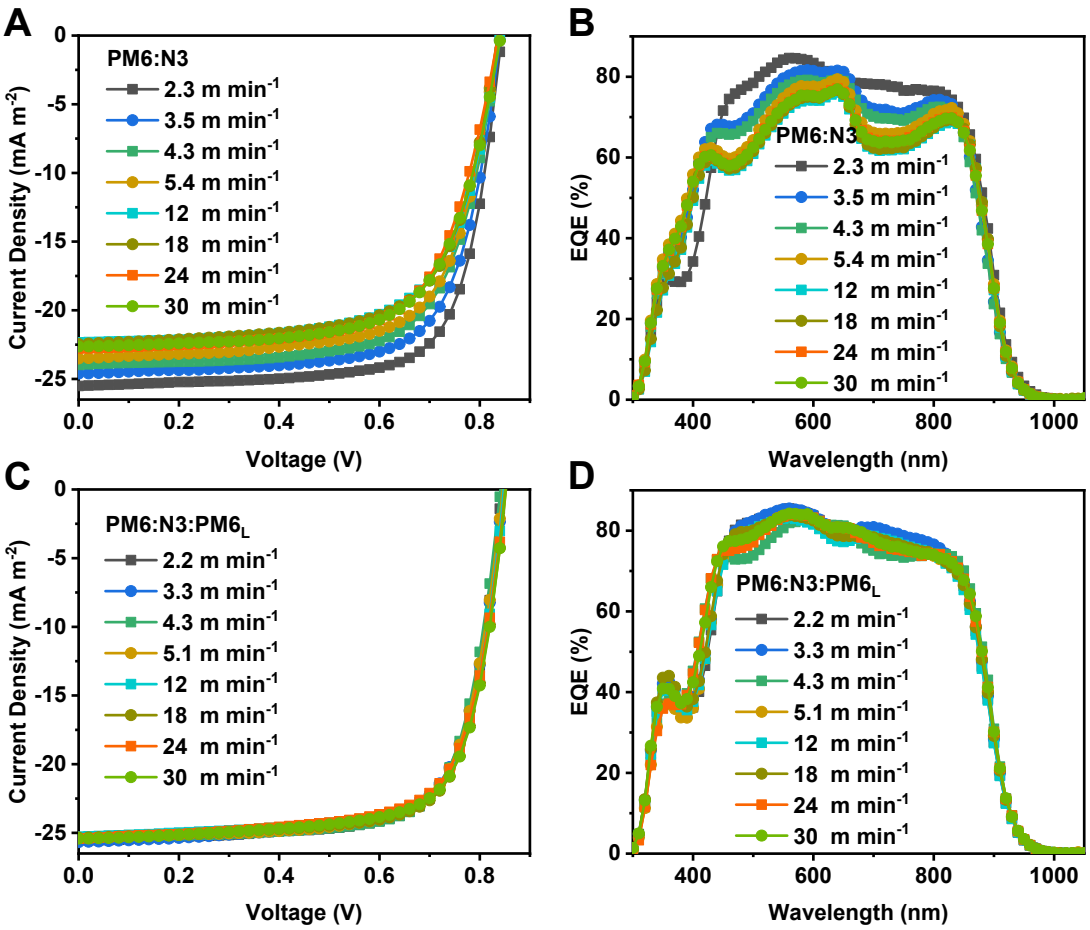

Figure S21. *J–V* characteristics of (A) dopant-free and (C) $PM6_L$-doped PM6:N3 systems OSCs with maximum PCE on different solution concentrations under constant incident light intensity (AM 1.5 G, 100 mW cm^{-2}), and the corresponding EQE spectra for (B) dopant-free and (D) $PM6_L$-doped devices.

Table S9. Photovoltaic parameters of PM6: N3 (5 wt% $PM6_L$) devices with different blade-coating speeds.

Active layer	Concentration /Speed [mg/mL]/ [m/min]	Thickness [nm]	V_{oc} [V]	J_{sc} [mA cm^{-2}]	$J_{sc\ cal.}$[a] [mA cm^{-2}]	FF [%]	PCE[b] [%]
PM6: N3	14.0/ 2.3	102	0.843	25.51	24.93	72.93	15.69 (15.57±0.10)
	12.0/ 3.5	97	0.841	24.61	23.92	70.68	14.63 (14.50±0.11)
	10.0/ 4.3	106	0.839	23.98	23.27	69.13	13.91 (13.81±0.07)
	8.0/ 5.4	101	0.836	23.51	22.88	68.50	13.47 (13.38±0.06)
	6.8/ 12.0	99	0.839	22.34	21.76	67.25	12.61 (12.49±0.08)
	6.5/ 18.0	96	0.836	22.45	21.88	67.71	12.71 (12.51±0.15)
	6.3/ 24.0	110	0.837	22.79	22.21	66.88	12.76 (12.62±0.11)
	6.0/ 30.0	104	0.842	22.64	22.11	67.13	12.76 (12.64±0.10)
PM6: N3: 5 wt% $PM6_L$	14.0/ 2.2	108	0.843	25.54	25.05	73.15	15.75 (15.57±0.14)
	12.0/ 3.3	105	0.846	25.66	25.32	71.65	15.55 (15.40±0.12)
	10.0/ 4.3	102	0.841	25.28	24.70	73.83	15.70 (15.59±0.09)
	8.0/ 5.1	98	0.846	25.34	24.72	73.03	15.66 (15.57±0.08)
	6.8/ 12.0	97	0.848	25.28	24.60	72.89	15.63 (15.51±0.08)
	6.5/ 18.0	112	0.852	25.36	24.85	73.31	15.84 (15.71±0.10)
	6.3/ 24.0	109	0.851	25.43	24.95	71.52	15.51 (15.36±0.12)
	6.0/ 30.0	95	0.852	25.42	25.07	72.65	15.73 (15.60±0.11)

[a] $J_{sc\ cal}$ represents the integrated current density obtained from EQE spectra. [b] The values in the bracket are the average PCE obtained from eight devices.

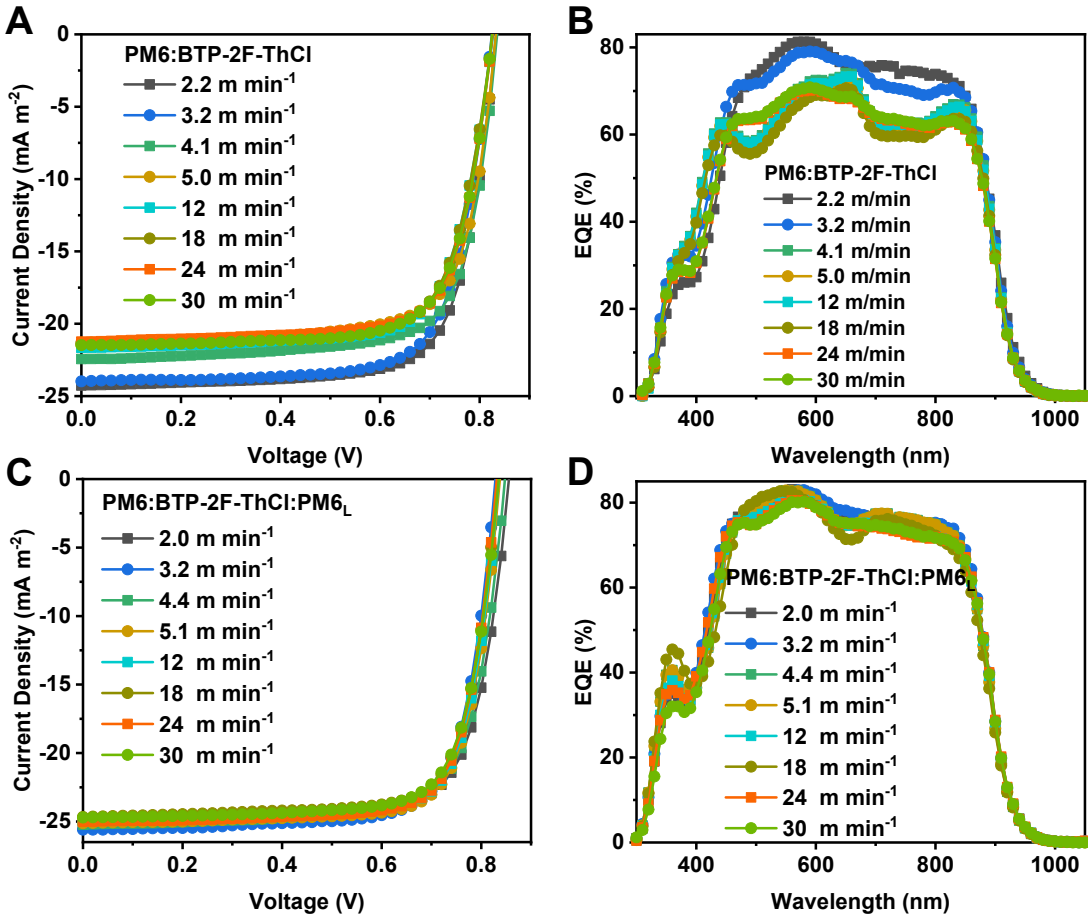

Figure S22. *J–V* characteristics of (A) dopant-free and (C) $PM6_L$-doped PM6:BTP-2F-ThCl systems OSCs with maximum PCE on different solution concentrations under constant incident light intensity (AM 1.5 G, 100 mW cm^{-2}), and the corresponding EQE spectra for (B) dopant-free and (D) $PM6_L$-doped devices.

Table S10. Photovoltaic parameters of PM6: BTP-2F-ThCl (5 wt% $PM6_L$) devices with different blade-coating speeds.

Active layer	Concentration /Speed [mg/mL]/ [m/min]	Thickness [nm]	V_{oc} [V]	J_{sc} [mA cm^{-2}]	$J_{sc\ cal.}$[a] [mA cm^{-2}]	FF [%]	PCE[b] [%]
PM6: BTP-2F-ThCl	14.0/ 2.2	102	0.833	24.27	23.62	74.09	14.98 (14.84±0.10)
	12.0/ 3.2	96	0.824	23.97	23.25	73.60	14.55 (14.41±0.10)
	10.0/ 4.1	115	0.835	22.42	21.33	73.99	13.85 (13.70±0.13)
	8.0/ 5.0	106	0.832	21.44	21.02	73.13	13.05 (12.95±0.07)
	6.8/ 12.0	98	0.827	21.66	21.14	73.42	13.15 (13.09±0.05)
	6.5/ 18.0	112	0.826	21.31	20.80	74.14	13.05 (12.91±0.10)
	6.3/ 24.0	105	0.826	21.24	20.69	74.34	13.04 (12.87±0.15)
	6.0/ 30.0	94	0.825	21.48	20.82	73.59	13.04 (12.90±0.10)
PM6: BTP-2F-ThCl: 5 wt% $PM6_L$	14.0/ 2.0	106	0.856	25.35	24.52	74.08	16.07 (15.97±0.07)
	12.0/ 3.2	111	0.829	25.59	24.60	75.31	15.97 (15.80±0.14)
	10.0/ 4.4	106	0.848	25.23	24.31	74.39	15.91 (15.74±0.15)
	8.0/ 5.1	95	0.837	25.12	24.26	76.68	16.13 (15.98±0.12)
	6.8/ 12.0	109	0.835	24.94	23.90	76.58	15.94 (15.81±0.10)
	6.5/ 18.0	121	0.833	24.66	23.79	76.30	15.67 (15.55±0.09)
	6.3/ 24.0	118	0.831	25.01	23.90	76.53	15.91 (15.72±0.14)
	6.0/ 30.0	107	0.835	24.71	23.74	75.59	15.60 (15.46±0.11)

[a] $J_{sc\ cal}$ represents the integrated current density obtained from EQE spectra. [b] The values in the bracket are the average PCE obtained from eight devices.

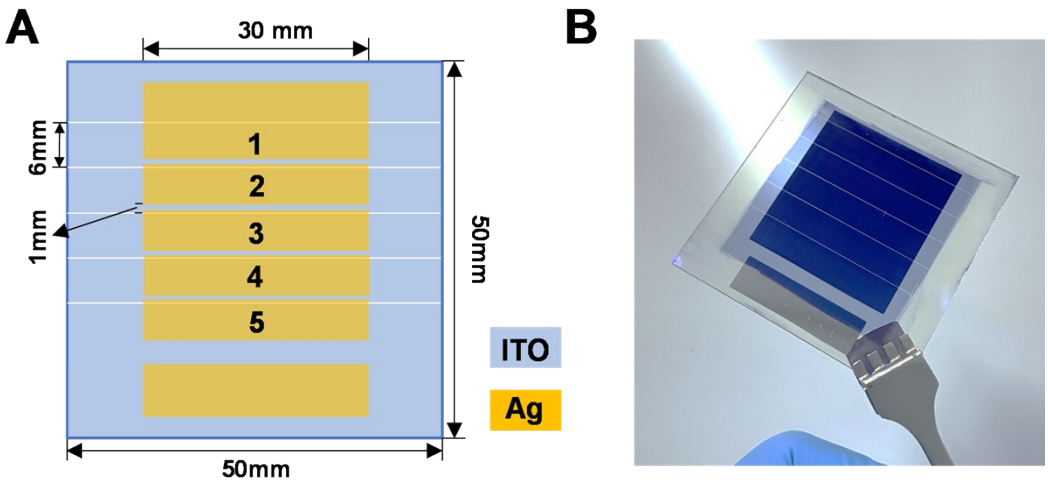

Figure S23. (A) The real configuration of the investigated solar modules based on five series-connected single cells of 5 mm × 30 mm. The total device area is 9.0 cm^2, and the active area is 7.5 cm^2. (B) The picture of large-scale module.

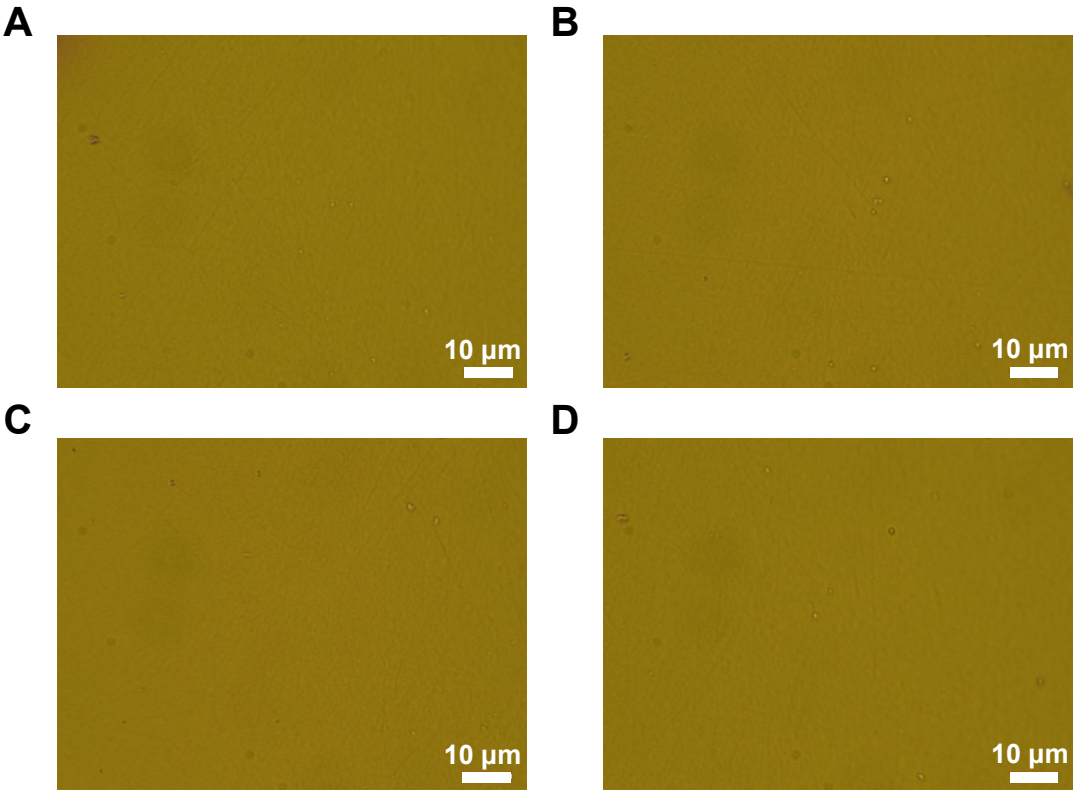

Figure S24. (A)-(D) optical microscopy images of four different spots of the large area photoactive layer films (PM6:Y6) fabricated at 2.3 m min^{-1}, respectively.

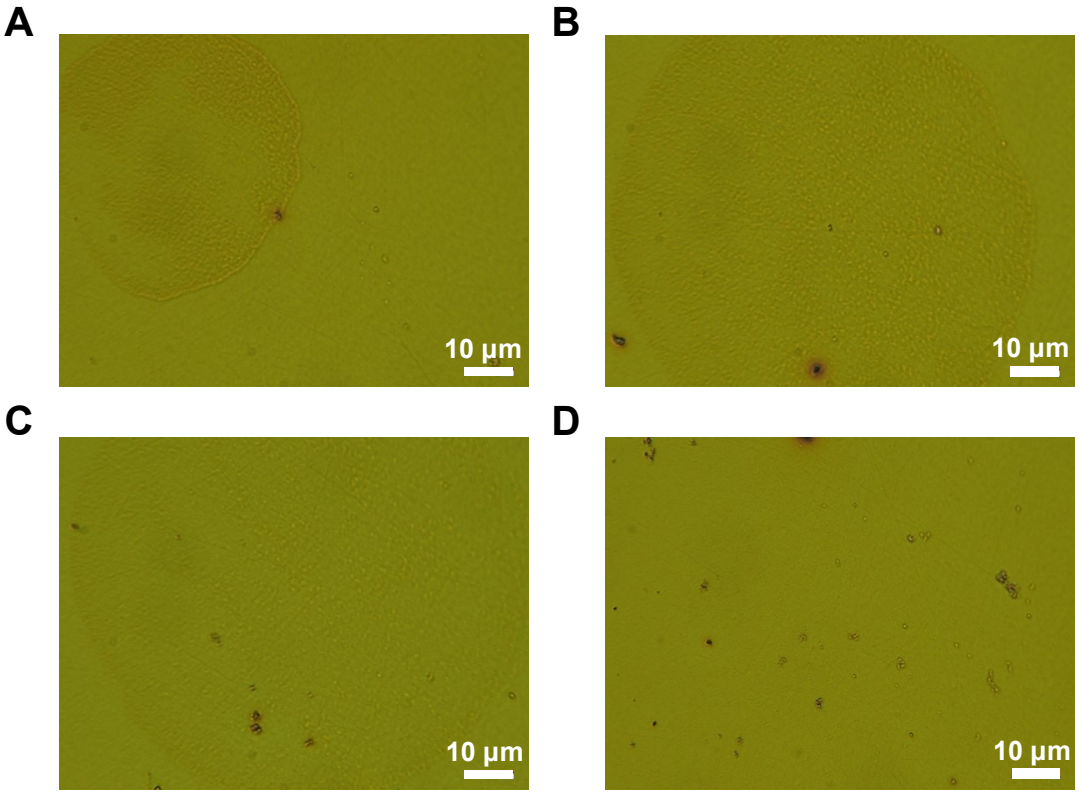

Figure S25. (A)-(D) optical microscopy images of four different spots of the large area photoactive layer films (PM6:Y6) fabricated at 30.0 m min^{-1}, respectively.

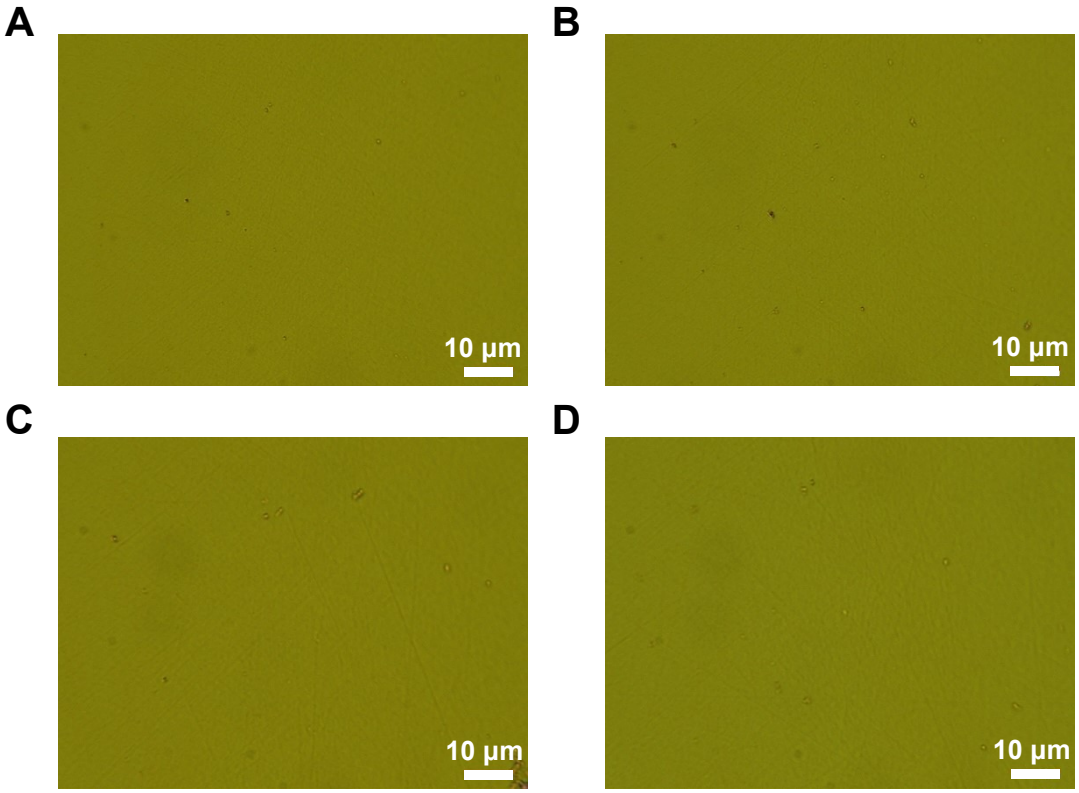

Figure S26. (A)-(D) optical microscopy images of four different spots of the large area photoactive layer (PM6:Y6:$PM6_L$) films fabricated at 30.0 m min^{-1}, respectively.